Mass separated particle flux from a laser-ablation metal cluster source

Yuta Ishikawa[1] , Jun Hasegawa[1] and Kazuhiko Horioka[2]

[1]Tokyo Institute of Technology, Ookayama Meguro-ku, Tokyo 152-8550, Japan and [2]KEK, Tsukuba, Ibaraki 305-0801, Japan

Abstract

Flux waveforms of aluminum cluster beams supplied from a laser-ablation cluster source were precisely investigated under various source conditions such as background pressure, ablation laser intensity, and nozzle structure. A time-of-flight mass spectroscopy revealed that aluminum clusters with sizes up to 200 were generated and the amount of the clusters could be maximized by choosing a proper background pressure ($\sim$2 MPa) and an ablation laser fluence ($\sim$40 mJ/cm^2). Flux waveforms of clusters having specific sizes were carefully reconstructed from the observed mass spectra. It is found that the pulse widths of the aluminum cluster beams were typically about 100 µs and much smaller than that of the monoatomic aluminum beam, indicating that the cluster formation was limited in a relatively small volume in the laser-ablated vapor. Introducing a conical nozzle having a large open angle was also found to enhance the cluster beam velocity and reduce its pulse width. A velocity measurement of particles in the cluster beam was conducted to examine the velocity spread of the supplied clusters. We found that the aluminum clusters were continuously released from the source for about 100 µs and this release time mainly determined the pulse width of the cluster beam, suggesting that controlling the behavior of an ablated vapor plume in the waiting room of the cluster source holds the key to drastically improving the cluster beam flux.

Introduction

When a large cluster ion such as C_{60} is injected into a solid material, a coincident impingement of multiple atoms composing the cluster induces unique phenomena such as crater formation (Tomaschko *et al.*, 1995; Yamada *et al.*, 2001), an enhancement of sputtering yield (Hasselkamp and Scharmann, 1983; Brunelle *et al.*, 2001), and an increase of stopping power (Ray *et al.*, 1992; Baudin *et al.*, 1994; Narumi *et al.*, 1998). Although a lot of studies on the irradiation effect of high-energy cluster ions have so far been conducted (Dammak *et al.*, 1995; Brunelle *et al.*, 1999; Tomita *et al.*, 2010), beam energies per nucleon were typically limited to less than 100 keV/u because of the upper limit of the acceleration voltage of electrostatic accelerators. To achieve higher cluster beam energy, Takayama *et al.* have recently proposed the concept of the induction microtron, which is designed to accelerate large cluster ions from 1 keV/u to more than 1 MeV/u without limitation on mass to charge ratios (Takayama *et al.*, 2007, 2015; Dixit *et al.*, 2009). Studies on cluster–material interaction in a more broad energy range are expected to be realized by the induction microtron in the near future.

The induction microtron requires injection of a pulsed cluster ion beam with a pulse duration of typically a few microsecond. Moreover, the input beam current needs to be high enough to obtain a reasonable amount of output cluster ions because charge exchange reactions between cluster ions and residual gas molecules probably cause considerable beam loss in the accelerator. Laser-ablation cluster sources have frequently been used to produce clusters of metals, semiconductors or alloy materials and to investigate physical properties (Brucat *et al.*, 1986; Ganteför *et al.*, 1988; Bucher *et al.*, 1991) and chemical reactions (Morse *et al.*, 1985; Whetten *et al.*, 1985; Alford *et al.*, 1986) of clusters. A combination of laser ablation and supersonic expansion of high-pressure buffer gas is preferable to produce a short-pulsed intense cluster beam with high directivity. Smalley and coworkers developed a laser-ablation cluster source for the first time to produce an intense beam of small aluminum clusters composed of less than 20 atoms (Dietz *et al.*, 1981). Rohlfing *et al.* introduced a waiting room to their cluster source, which drastically promoted the growth of clusters, and showed that large carbon clusters composed of more than hundreds of atoms were produced (Rohlfing *et al.*, 1984). Milani *et al.* succeeded in enhancing cluster production by employing a laser-incident channel having a large diameter, which allows them to irradiate the target with a large laser spot and enhance the vapor production (Milani and deHeer, 1990). Most of these studies have been dedicated to examine the mass spectrum and the yield of generated clusters. On the other hand, the flux waveforms of cluster beams available from a laser-ablation cluster source have not so far been studied sufficiently.
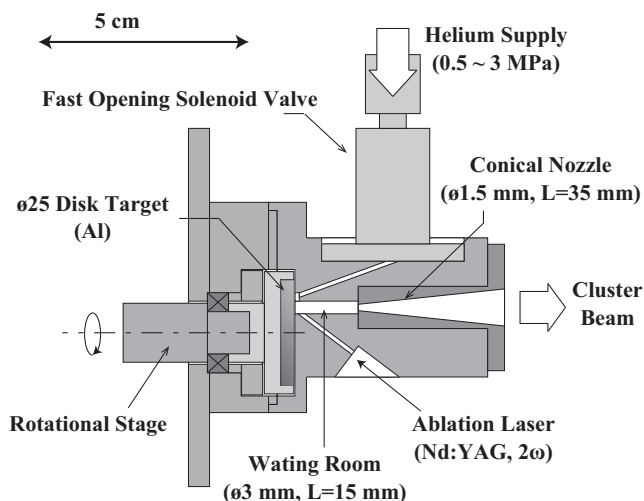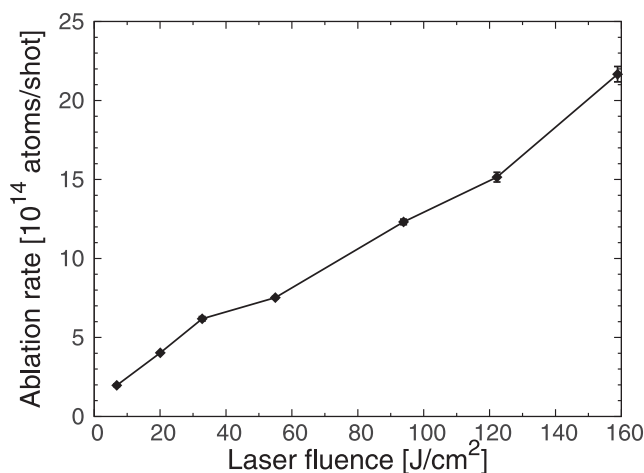
Fig. 1. The cross-sectional view of the laser-ablation-type cluster source developed in this study.

Fig. 2. Dependence of the ablation rate (the number of atoms evaporated per a laser shot) on the laser fluence.

The purpose of this study is to explore the intensity of cluster beams supplied by a laser-ablation cluster source and provide strategies for improving cluster beam flux. The generation and growth of clusters depends on the clustering process, which is closely related to the history of the density and temperature of the laser-ablated vapor plume. The transportation process, in which the ablation vapor containing cluster particles is ejected together with a supersonic helium gas flow through a nozzle, also affects finally available cluster beam fluxes. We investigate the beam fluxes of aluminum atoms and clusters supplied from a laser-ablation cluster source under various operational conditions (backing helium pressure, laser fluence, and nozzle shape), and discuss how these parameters affect the cluster generation and transportation processes.

Experimental setup

Figure 1 shows the geometry of the laser-ablation cluster source developed in this study. A frequency-doubled Nd:YAG laser (λ = 532 nm, 5 ns FWHM, 5 Hz) irradiated an aluminum disk target ($\varnothing$25 mm) mounted on a motorized rotational stage. The laser spot on the target surface has an elliptical shape ($0.1 \times 0.05\pi$ mm^2). The ablation laser fluence (I_A) was changed in the range of 5–200 J/cm^2 by controlling the Q-switch delay time. The ablation rate of aluminum atoms, which was measured from the mass reduction of the Al target after 10^5 laser shots, linearly increased with increasing laser fluence as shown in Figure 2. The rotation speed of the target was set to ~20 rpm to avoid the overlap of successive laser shots, leading to good reproducibility of laser ablation. Pulsed helium gas was supplied through a fast opening solenoid valve (open time ~1.5 ms) with a backing pressure (P_{He}) ranging from 0.5 to 3 MPa. To perform laser ablation after helium gas completely filled a waiting room ($\varnothing$3 mm, L = 15 mm), the time interval between the onset of valve opening and the laser irradiation was fixed to 800 μs. Metal vapor produced by laser irradiation was carried into vacuum through a conical nozzle by a supersonic helium gas flow. A conical nozzle with a throat diameter of 1.5 mm and an open angle of 6° was normally used in this experiment. In addition to this nozzle, a conical nozzle with a different open angle (3°) and a straight nozzle with a

throat diameter of 2 mm were also used to examine the nozzle shape effect on the cluster beam flux. All these nozzles have a length of 3.5 cm.

The whole experimental setup is shown in Figure 3. A voltage of 500 V was applied to deflection plates (A) at the outlet of the cluster source to eliminate charged particles and observe only neutral particles downstream. Two skimmers ($\varnothing$1.5 and $\varnothing$3) and an aperture ($\varnothing$3 mm) were coaxially aligned on the beam axis to collimate the cluster beam. A two-stage differential pumping keeps the pressure in the analysis region at ~5×10^{-5} Pa. The distance between the outlet of the cluster source and the skimmer was 7.4 cm. A time of flight mass spectrometer (TOFMS) was located 60 cm downstream from the nozzle exit. An ArF excimer laser (λ = 193 nm, 30 ns FWHM, 5–200 μJ) was used to irradiate a 1 mm × 1 mm area in the acceleration gap of the TOFMS to ionize the clusters. The photon energy of the ArF excimer laser (6.4 eV) is high enough to ionize aluminum atoms and clusters (Al$_N$, $N \geqslant 14$) by a single photon process (Schriver et al., 1990). The interval between the ablation laser irradiation and the ionization laser irradiation (τ_D) was precisely controlled by a pulse delay generator. Ionized clusters were orthogonally accelerated by two-stage acceleration gaps (20 kV in total) and finally focused onto a micro channel plate (MCP) by an einzel lens. To observe relatively small signals of the clusters, a voltage of 500 V was applied to deflection plates (B) behind the acceleration gap to eliminate monoatomic ions and prevent them from disturbing the sensitive measurement of the cluster signals.

Figure 4 shows the survival rates of the cluster ions having initial velocities of 750–2500 m/s in the direction of the cluster beam axis. These survival rates were evaluated by precise particle trajectory calculations in the TOF system. As shown in the figure, heavy cluster ions with relatively high-initial velocities are partly lost during the flight toward the detector because the deflection of these particles is insufficient owing to their large inertia. In contrast, small cluster ions with relatively small initial velocities are also lost because of excessive deflection. One can see that cluster ions with sizes of 50–100 and initial velocities of 1000–2000 m/s can be detected with high efficiency (~100%). Of course, the survival rate varies depending on the deflection voltage, but we fixed it to be 500 V because we focus on the clusters with sizes of ~50–100. The MCP signal was averaged over 64–512 shots to reduce statistical errors and increase signal to noise ratios.
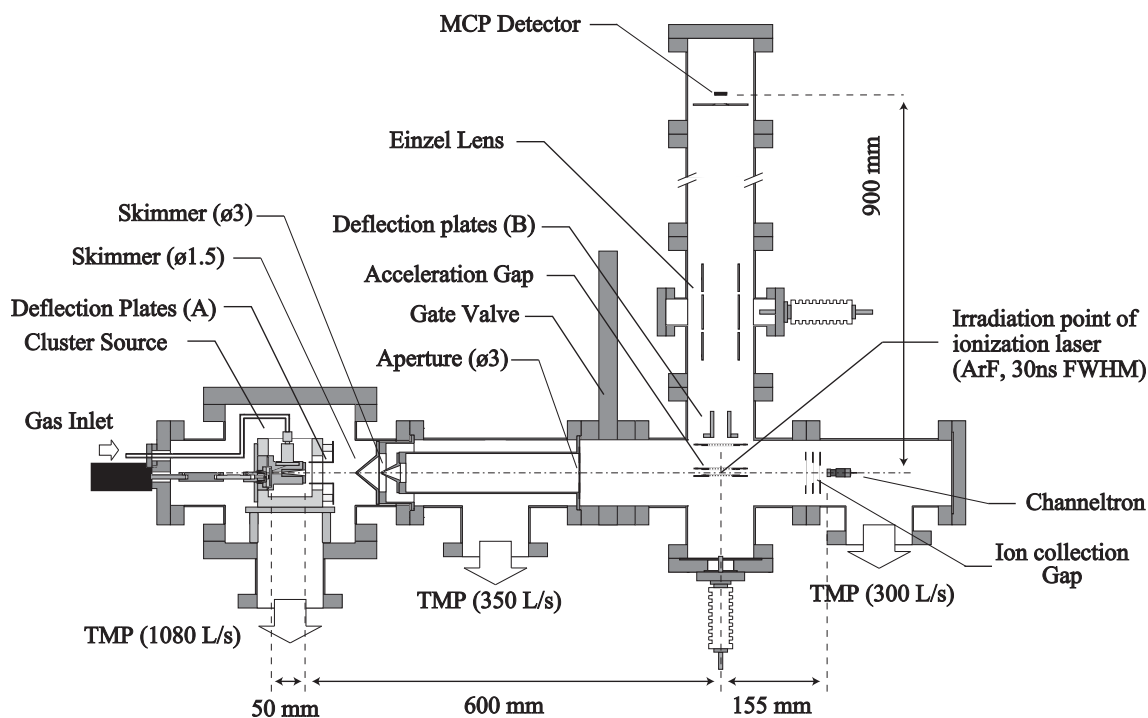
Fig. 3. A schematic of the experimental setup of the TOFMS and the particle velocity measurement.
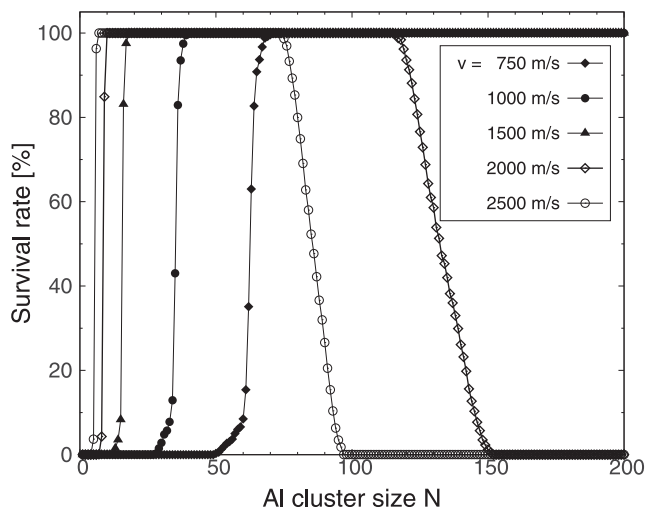

Fig. 4. The survival rate of Al cluster ions with various initial velocities. The voltage applied to the deflection plate (B) is fixed at 500 V.
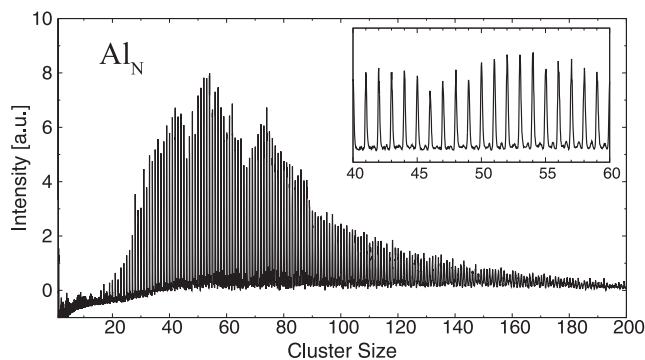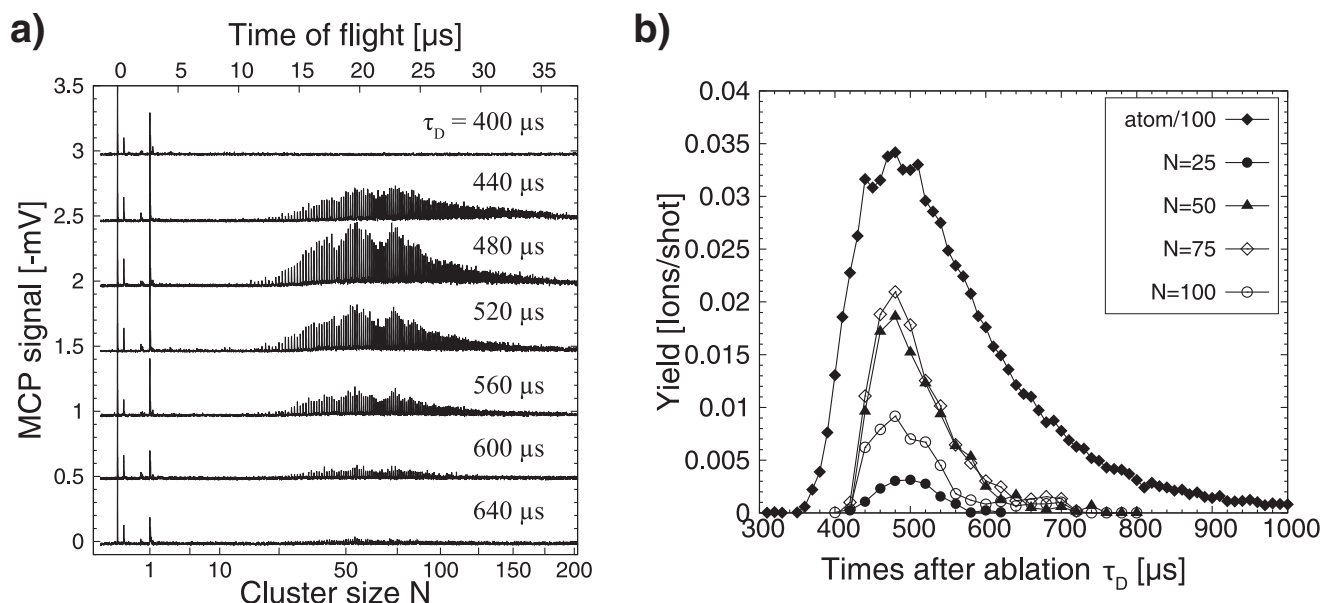

Fig. 5. A typical mass spectrum of Al_N clusters obtained by TOFMS. A detailed spectrum in a size range from 40 to 60 is also shown in the inserted figure. The ablation laser fluence (I_A) was 130 J/cm^2 and the ionization laser fluence (I_I) was 0.6 mJ/cm^2, PHe = 2.0 MPa. τ_D = 460 μs.

Result and discussion

Figure 5 shows a typical mass spectrum of aluminum clusters observed with an ablation laser fluence of 130 J/cm^2. The ionization laser fluence was small (0.6 mJ/cm^2) enough to prevent the distortion of the mass spectrum due to the photo-dissociation of large clusters. Signals of Al_N clusters with sizes up to 200 were observed. The mass spectrum had gentle peaks around $N = 40$, 55, and 65. Small clusters ($N < 15$) were not observed because they were largely attenuated by the deflection (see Fig. 4). The inserted figure shows a detailed spectrum of the clusters with sizes of 40–60. Although small peaks of aluminum cluster oxide ($Al_N O$) can be seen between the peaks of Al_N clusters, their intensities were much smaller than those of the Al_N clusters, which indicates that the impurities in the supplied helium gas were negligibly small and not harmful in the cluster growth process.

The velocities of the cluster particles were also measured using an ion detector located on the beam axis 75.5 cm downstream from the cluster source outlet. The detector consisted of ion collection electrodes and a Channeltron. In this measurement, the ArF excimer laser irradiated the center of the acceleration gap of the TOFMS system to ionize neutral particles, but no acceleration voltage was applied to the gap. The ionized particles passed through the gap and reached the Channeltron after being slightly accelerated and focused by the ion collection electrodes and the Channeltron biased to −100 V in total. We evaluated the velocities of the particles from their time of flights (TOFs) from the ionization point to the Channeltron.

a)

b)

Fig. 6. (a) TOF signals observed with τ_D = 400–640 μs. I_A = 130 J/cm², I_I = 0.6 mJ/cm², and P_{He} = 2.0 MPa. (b) Reconstructed flux waveforms of Al atoms and clusters (N = 25, 50, 75, and 100).

TOF signals observed under various delays of the ionization laser (τ_D) are compared in Figure 6(a). The shape of the TOF signal was almost independent of τ_D. The flux waveform of specific size clusters was reconstructed from the TOFMS signals by examining the temporal change of the intensity of the corresponding mass peak. The reconstructed flux waveforms of aluminum atoms and clusters (N = 25, 50, 75, and 100) are shown in Figure 6(b). The yield on the vertical axis was converted from the peak intensity assuming that the MCP gain was 5×10^7 irrespective of the cluster ion mass. Note that the yield of the Al atoms is artificially attenuated by 10^{-2} in this figure. The arrival time of the Al atoms ranged from 300 μs to 1000 μs and the flux peaked at τ_D ~500 μs. The fluxes of the Al_N clusters also peaked at the same time, but had narrower pulse durations (~100 μs FWHM) than that of the Al atoms (~200 μs FWHM).

The horizontal axis in Figure 6(b) represents the elapsed time from the time (τ_D = 0) at which the target was irradiated with the ablation laser. From the figure, one can see that it takes about 500 μs for the particles constituting the peak of the flux waveform to reach the irradiation point of the ionizing laser (see Fig. 3) after they were generated by laser ablation. However, this result does not necessarily mean that these particles have the same velocity as that obtained by dividing the flight distance (~650 mm) by the arrival time (500 μs). Since the ablation vapor stagnates in the waiting room while mixing with helium gas and then flows through the narrow nozzle throat, the particles expelled from the nozzle at a given moment could generally have different velocities.

To experimentally confirm this, we measured particle velocity using a Channeltron detector located downstream of the TOFMS system. Figure 7 shows the output signal waveforms of the Channeltron obtained while changing the irradiation timing of the ionization laser (τ_D). The horizontal axis represents the TOF from the ionization location of aluminum atoms and clusters by the ArF excimer laser to the Channeltron (upper axis) and the particle velocity (bottom axis) converted from the TOF by taking into account the acceleration of ions by electric fields induced by the collection electrodes and the Channeltron itself. The diagonal
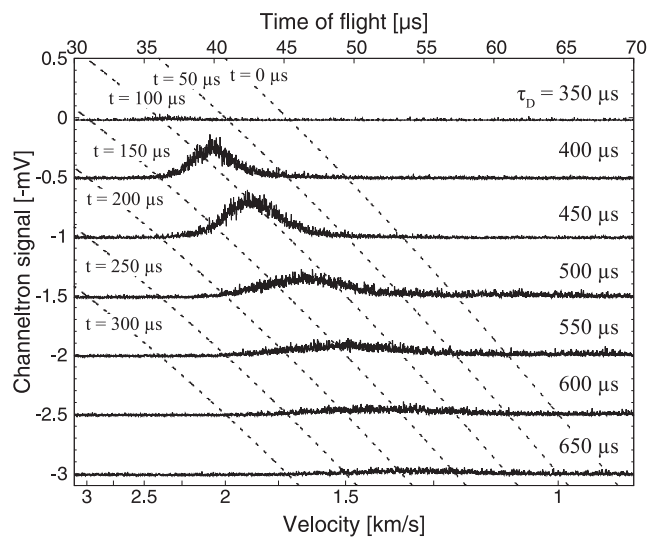

Fig. 7. Time-of-flight signals acquired by particle velocity measurement. Signals were averaged over 512 shots. Dashed lines represent the particle release time t at which particles leave the nozzle outlet (t = 0 corresponds to the ablation laser irradiation). I_A = 130 J/cm², I_I = 2.6 mJ/cm², and P_{He} = 2.0 MPa.

dashed lines in the figure denote the times when the particles were emitted from the nozzle, which were inversely calculated for typical particle velocities. For example, when τ_D = 400 μs, a peak of the signal appears 40 μs after ionizing laser irradiation, meaning that the average velocity of the particles passing through the ionization point at this moment (τ_D = 400 μs) was ~2.1 km/s. From the width of the signal waveform and the diagonal dashed line, we found that these particles were emitted from the nozzle of the cluster source between t = 50 μs and 150 μs after the ablation laser irradiation. This result shows that the slower particles (~1.6 km/s) released from the nozzle at earlier time (t ~ 50 μs) and faster particles (~2.5 km/s) released at later time (t ~ 150 μs) reached the ionization point at the same time.
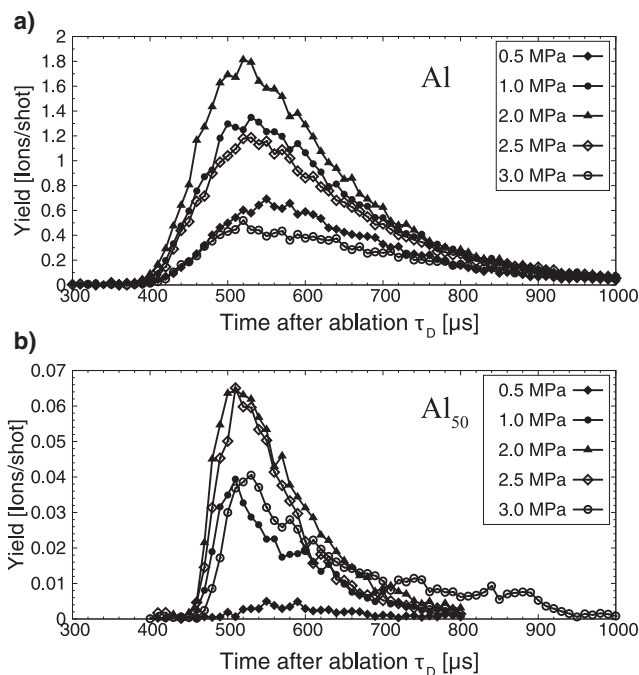
Fig. 8. Backing pressure dependences of flux waveforms of (a) Al and (b) Al_{50}. I_A = 130 J/cm², I_I = 0.6 mJ/cm².
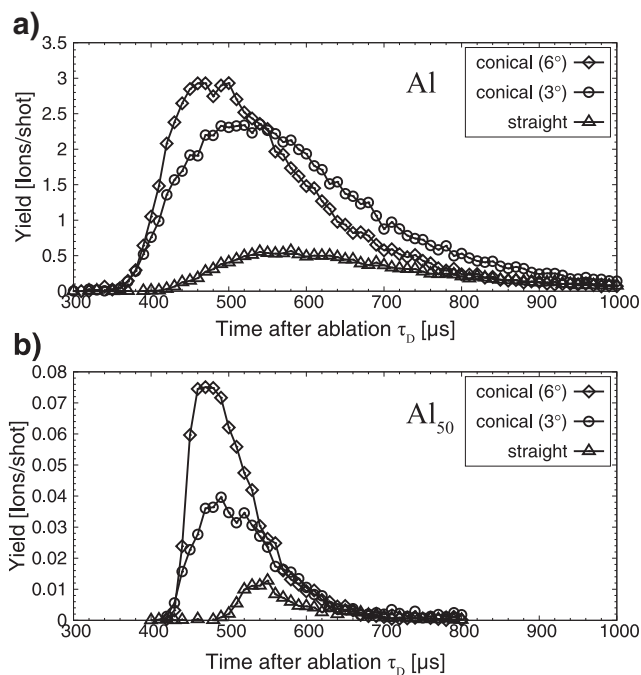
Fig. 9. Dependence of Al and Al_{50} beam flux waveforms on the nozzle shape. Two conical nozzles with different open angles (6° and 3°) and a straight nozzle were used. I_A = 130 mJ/cm², I_I = 0.6 mJ/cm², and P_{He} = 2 MPa.

Hereafter, we call the time that it takes for the particles such as atoms and clusters to be released from cluster sources "particle release time". The waveforms for other delay times (τ_D) have the similar tendencies, but we found that the average velocity of the detected particles gradually decreased with τ_D. It was also found that the width of the signal, that is the velocity spread of the particles, increased with τ_D.

Here, again, let us focus on the flux waveforms in Figure 6(b). The average velocity of the particles constituting the peak of the aluminum atomic beam is estimated to be ~1.7 km/s from the waveform of τ_D = 500 μs in Figure 7, which is slightly higher than the sound velocity of helium (~1.0 km/s at 300 K). This result supports that the aluminum atoms generated by laser ablation were accelerated and transported downstream by the supersonic helium flow formed by the nozzle. On the other hand, the velocity spread of these particles evaluated from the FWHM of the signal waveform in Figure 7 was about ± 0.1 km/s. Since the distance from the nozzle outlet to the ionizing laser irradiation position is 600 mm, the time spread of the flux waveform caused by this velocity spread is estimated to be about 50 μs. As discussed above, considering that it takes about 50–150 μs for the particles to be released from the cluster source, we can roughly explain the observation result that the flux waveform of the aluminum atom had a width of about 200 μs by the velocity spread and the particle release time. Since the particle velocity spread depends mainly on the temperature of the ablated aluminum vapor, it is not easy to reduce it. On the other hand, the particle release time may be significantly shortened if the metal vapor generated by laser ablation can be quickly transported to the nozzle while confining it with high-pressure helium gas and keeping its volume quite small.

From the flux waveforms of the cluster beams in Figure 6(b), it can be seen that their pulse widths (FWHM) were much smaller than that of aluminum atoms. Assuming that cluster particles of different sizes are in equilibrium with each other and have the

same temperature, the velocity spread of the cluster particles should decrease with its size (mass). The experimental result that the pulse width of the cluster beam was independent of the size indicates that what mainly determines the pulse width of the cluster beam flux is not the velocity spread of cluster particles, but the particle release time. Cluster formation does not necessarily occur in the entire volume of the aluminum vapor plume, but is generally limited to a region where thermodynamical conditions suitable for atomic aggregation hold. Therefore, it is reasonable that the particle release time of clusters was much smaller than that of aluminum atoms, resulting in the shorter pulse length of the cluster beams.

Backing pressure dependences of the beam fluxes of Al and Al_{50} are presented in Figure 8(a) and (b), respectively. The largest fluxes were obtained with a backing pressure of 2 MPa for both Al and Al_{50}. This result indicates that when $P_{He} \leqslant 2$ MPa, the increase in the backing pressure improved the transport efficiency of the aluminum vapor containing clusters. On the other hand, when $P_{He} > 2$ MPa, the increase in the residual gas pressure in the chamber probably disturbs and decelerates the supersonic helium gas flow and largely reduces the transport efficiency of the particles. The deceleration of the supersonic jet can be minimized by shortening the distance between the nozzle outlet and the skimmer or intensifying the evacuation speed. As shown in Figure 8(b), the tail of the Al_{50} flux waveform observed with a backing pressure of 3 MPa is much longer than those with lower pressures. This result implies that the cluster condensation efficiency was enhanced by the strong confinement of the metal vapor in high-pressure helium gas, leading to the increase in the total amount of clusters.

Figure 9 compares the flux waveforms of Al and Al_{50} observed with two conical nozzles and a straight nozzle. In both cases of Al and Al_{50}, the particle fluxes were largely enhanced by the conical nozzles. As for the conical nozzles, more intense beam fluxes of
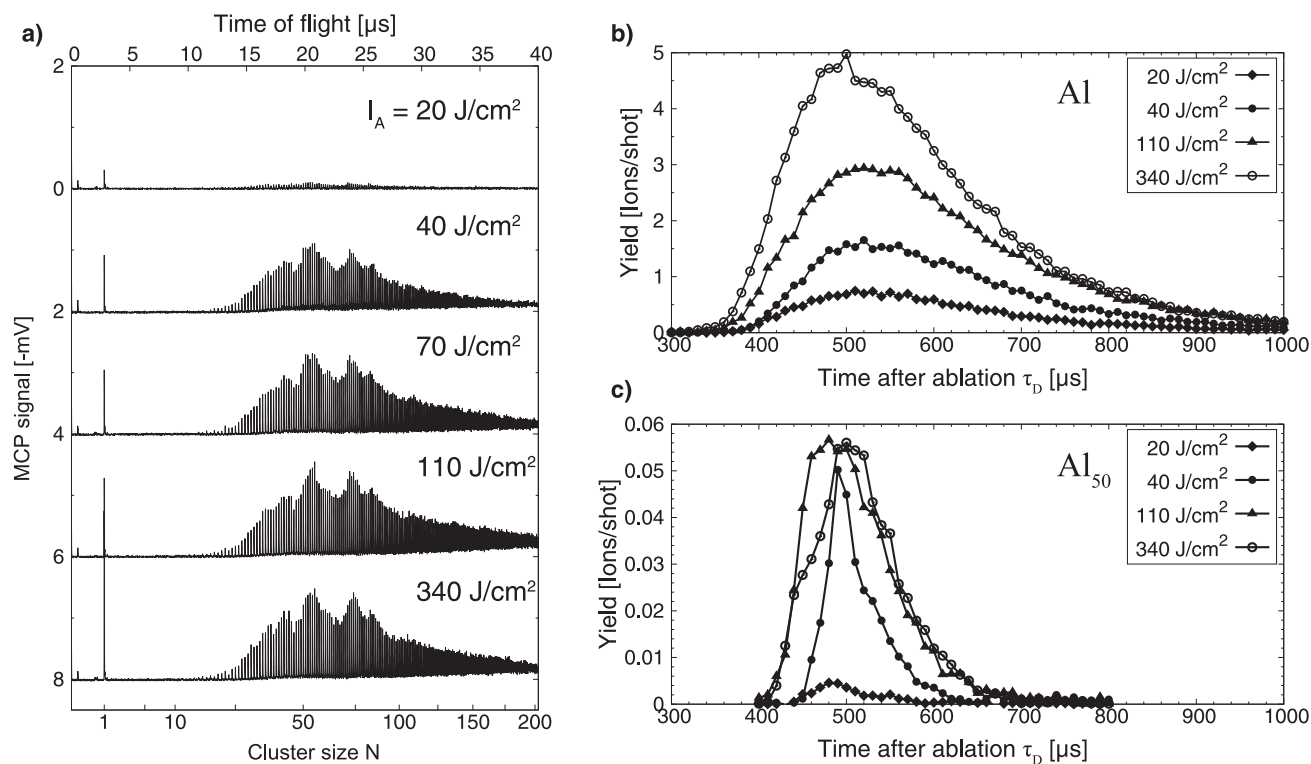
Fig. 10. Dependence of Al cluster generation on the ablation laser fluence I_A. $I_I = 0.6$ mJ/cm^2. $P_{He} = 2$ MPa. (a) TOF signals. $\tau_D = 500$ μs. (b) Flux waveforms of aluminum atom. (c) Flux waveforms of Al$_{50}$.

Al and Al$_{50}$ were obtained with a larger open angle (6°). This is probably because the Mach number of the jet (the directivity of particles) increased as the ratio of the cross-sectional area of the nozzle outlet (A) to that of the nozzle throat (A^*) increased. Assuming that the temperature of the helium gas in the waiting room is 300 K, the flow velocities at the nozzle outlet are calculated to be 1680 m/s and 1725 m/s, respectively for the 3° conical nozzle ($A/A^* \sim 12$) and the 6° conical nozzle ($A/A^* \sim 35$). For the conical nozzles, the flight time from the nozzle outlet to the TOFMS is ~350 μs, and considering that the particle release time was 50–150 μs, the arrival time of Al$_{50}$ is 400 to 500 μs, which is in good agreement with the experimental result.

TOF signals and flux waveforms of Al and Al$_{50}$ with different ablation laser fluences are compared in Figure 10. The aluminum atom flux increased with the ablation laser fluence as shown in Figure 10(b). This is clearly due to the enhancement of the amount of ablation vapor as shown in Figure 2. The Al$_{50}$ flux was drastically enhanced when the ablation laser fluence increases to 40 J/cm^2. However, when $I_A \geqslant 40$ J/cm^2, the amount and the size distribution of clusters hardly changed [Fig. 10(a)] and the peak values of the Al$_{50}$ cluster flux were almost the same as shown in Figure 10(c). This result suggests that the cluster formation and growth was suppressed by the temperature increase of the ablated vapor due to increased laser fluence.

The influence of the ionization laser fluence (I_I) on the cluster ion production is shown in Figure 11. The TOF signals of Al cluster ions shown in Figure 11(a) were slightly shifted to a lower side and the gentle peaks on the signals gradually disappears as the ionization laser fluence increases. This result shows that the photo-dissociation of clusters became remarkable when the

ionization laser fluence was increased. Small cluster ions ($N \leqslant 14$) observed under high-ionization laser fluences are probably the product of the photo-dissociation of large-cluster ions. Although the cluster beam flux increased with increasing the ionization laser fluence, the shape of the flux waveforms of Al$_{50}$ clusters was less sensitive to the fluence as shown in Figure 11(b). To compare the cluster ion production efficiency, total yields of clusters were evaluated by the time integration of the flux waveforms [Fig. 11(c)]. The total yields of aluminum atoms and clusters ($N = 50$ and 100) almost linearly increased with increasing laser fluence when $I_I \leqslant 10$ mJ/cm^2. When the ionization laser fluence exceeds 10 mJ/cm^2, the total yields of the aluminum atoms and relatively small clusters ($N = 14$) were largely enhanced probably due to the increase in the amount of photo-fragments. On the other hand, the total yield of large clusters ($N = 50$ and 100) saturated with laser fluences over 10 mJ/cm^2. The photoionization cross-section of aluminum atoms is ~50 Mb (0.5 Å^2) at a wavelength of ~193 nm (Kohl and Parkinson, 1973) and large aluminum clusters have larger photoionization cross-sections than this value. Thus, the observed saturation in the yield of the Al clusters may be due to that almost all the aluminum clusters were ionized under laser fluences over 10 mJ/cm^2 (~1 photon/Å^2).

In our cluster source the laser spot size was limited by the narrow-laser incident channel. Thus, increasing the ablation laser energy resulted in excess vapor heating. For increasing the cluster flux, it is probably effective to increase the spot size while maintaining the fluence. The pulse width of the cluster beam could be shortened by improving the cluster source structure so that the generated vapor can be transported to the nozzle in the waiting room while keeping the vapor volume small.
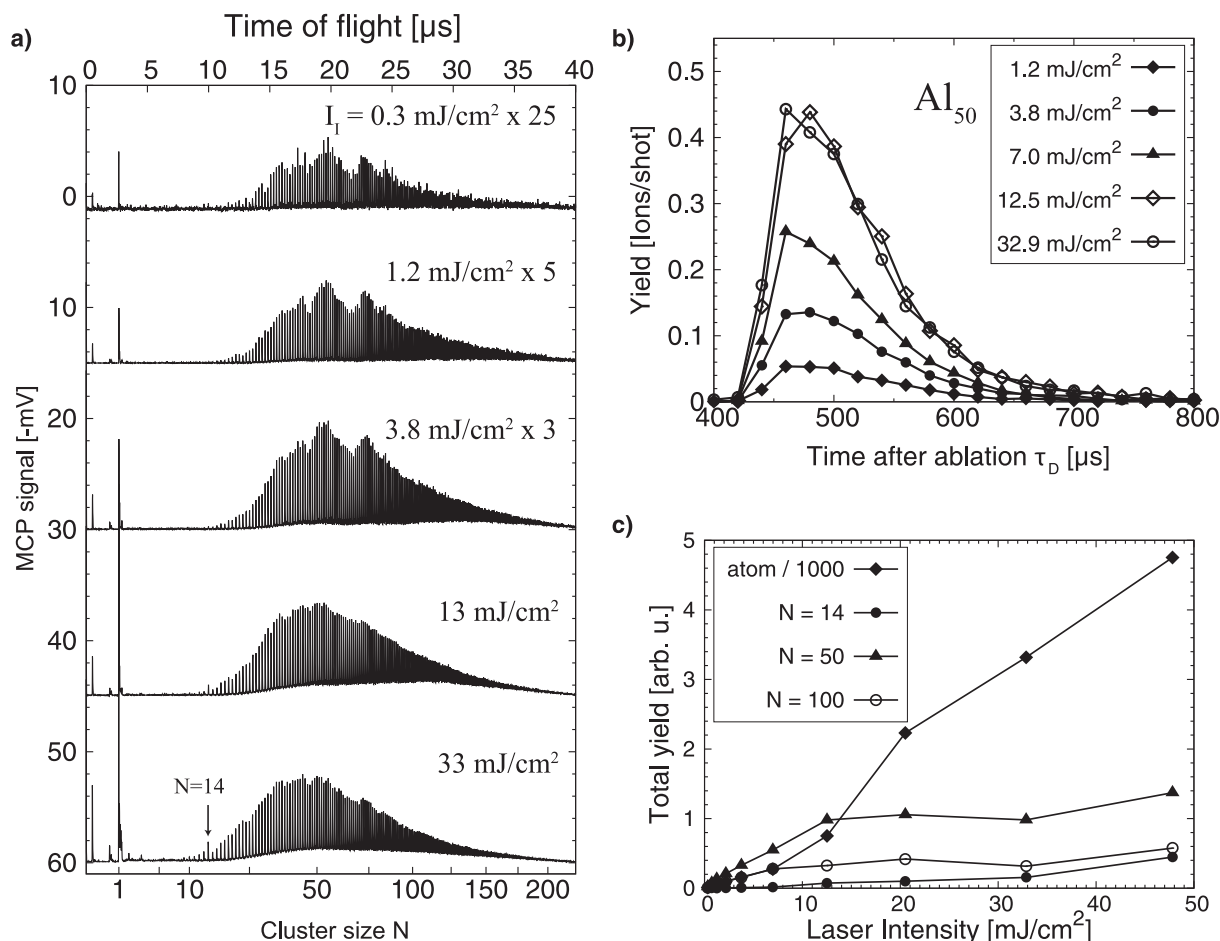
Fig. 11. Dependence of cluster ion production on the ionization laser fluence (I_I). I_A = 130 J/cm^2. P_{He} = 2.0 MPa. (a) TOF signals. These signals are normalized by the signal intensities. τ_D = 480 μs. (b) Flux waveforms of Al$_{50}$. (c) Total yields of each particle (aluminum atom and Al$_{14,50,100}$) obtained by the time integration of the flux waveform.

Conclusion

To design high-flux cluster beam sources required for high-energy circular cluster accelerators, we conducted an experimental survey on how the operational parameters of the laser-ablation cluster source affect the cluster size distribution and flux waveforms. We observed aluminum clusters with sizes up to 200 and found that the pulse width of the cluster beam was typically about 100 μs. Increasing the backing pressure enhanced the cluster generation and improved the transportation efficiency of the clusters. The nozzle shape also affected the cluster flux because the directivity of the cluster beam was determined by the acceleration in the nozzle. The largest cluster flux was obtained by the conical nozzle with an open angle of 6°. When the ablation laser intensity increased beyond 40 J/cm^2, the cluster flux saturated, which may be caused by an increase in the vapor temperature. Increasing the laser spot size while keeping the fluence is probably effective to enhance cluster production. The pulse width of the cluster beam was found to be about 100 μs, which is mainly determined by the particle release time from the source. To enhance the cluster beam flux, the correlation between the cluster source structure and the pulse width of the cluster beam should be investigated in more detail.

References

Alford JM, Weiss FD, Laaksonen RT and Smalley RE (1986) Dissociative chemisorption of molecular hydrogen on niobium cluster ions. A supersonic cluster beam FT-ICR experiment. *The Journal of Physical Chemistry* **90**, 4480–4482.

Baudin K, Brunelle A, Chabot M, Della-Negra S, Depauw J, Gardès D, Håkansson P, Beyec YL, Billebaud A, Fallavier M, Remillieux J, Poizat JC and Thomas JP (1994) Energy loss by MeV carbon clusters and fullerene ions in solids. *Nuclear Instruments and Methods in Physics Research Section B*: **94**, 341–344.

Brucat PJ, Zheng LS, Pettiette CL, Yang S and Smalley RE (1986) Metal cluster ion photofragmentation. *The Journal of Chemical Physics* **84**, 3078–3088.

Brunelle A, Della-Negra S, Depauw J, Jacquet D, Le Beyec Y and Pautrat M (1999) Reduced charge state of MeV carbon cluster constituents exiting thin carbon foils. *Physical Review A* **59**, 4456.

Brunelle A, Della-Negra S, Depauw J, Jacquet D, Le Beyec Y, Pautrat M, Baudin K and Andersen HH (2001) Enhanced secondary-ion emission under gold-cluster bombardment with energies from keV to MeV per atom. *Physical Review A* **63**, 022902.

Bucher JP, Douglass DC and Bloomfield LA (1991) Magnetic properties of free cobalt clusters. *Physical Review Letters* **66**, 3052.

Dammak H, Dunlop A, Lesueur D, Brunelle A, Della-Negra S and Le Beyec Y (1995) Tracks in metals by MeV fullerenes. *Physical Review Letters* **74**, 1135.

Dietz TG, Duncan MA, Powers DE and Smalley RE (1981) Laser production of supersonic metal cluster beams. *The Journal of Chemical Physics* **74**, 6511–6512.

Dixit TS, Iwashita T and Takayama K (2009) Induction acceleration scenario from an extremely low energy in the KEK all-ion accelerator. *Nuclear Instruments and Methods in Physics Research Section A: Accelerators, Spectrometers, Detectors and Associated Equipment* **602**, 326–336.

Ganteför G, Gausa M, Meiwes-Broer KH and Lutz HO (1988) Photoelectron spectroscopy of jet-cooled aluminium cluster anions. *Zeitschrift für Physik D Atoms, Molecules and Clusters* **9**, 253–261.

Hasselkamp D and Scharmann A (1983) Ion-induced electron emission from carbon. *Physica Status Solidi. A, Applied Research* **79**, K197–K200.

Kohl JL and Parkinson WH (1973) Measurement of the neutral-aluminum photoionization cross-section and parameters of the 3p 2PO-3s3p2 2S112 autoionization doublet. *The Astrophysical Journal* **184**, 641–652.

Milani P and deHeer WA (1990) Improved pulsed laser vaporization source for production of intense beams of neutral and ionized clusters. *Review of Scientific Instruments* **61**, 1835–1838.

Morse MD, Geusic ME, Heath JR and Smalley RE (1985) Surface reactions of metal clusters. II. Reactivity surveys with D2, N2, and CO. *The Journal of Chemical Physics* **83**, 2293–2304.

Narumi K, Nakajima K, Kimura K, Mannami MH, Saitoh Y, Yamamoto S, Aoki Y and Naramoto H (1998) Energy losses of B clusters transmitted through carbon foils. *Nuclear Instruments and Methods in Physics Research Section B: Beam Interactions with Materials and Atoms* **135**, 77–81.

Ray E, Kirsch R, Mikkelsen HH, Poizat JC and Remillieux J (1992) Slowing down of hydrogen clusters in thin foils. *Nuclear Instruments and Methods in Physics Research Section B: Beam Interactions with Materials and Atoms* **69**, 133–141.

Rohlfing EA, Cox DM and Kaldor A (1984) Production and characterization of supersonic carbon cluster beams. *The Journal of Chemical Physics* **81**, 3322–3330.

Schriver KE, Persson JL, Honea EC and Whetten RL (1990) Electronic shell structure of group-IIIA metal atomic clusters. *Physical Review Letters* **64**, 2539.

Takayama K, Arakida Y, Iwashita T, Shimosaki Y, Dixit T and Torikai K (2007) All-ion accelerators: An injector-free synchrotron. *Journal of Applied Physics* **101**, 063304.

Takayama K, Adachi T, Wake M and Okamura K (2015) Racetrack-shape fixed field induction accelerator for giant cluster ions. *Physical Review Special Topics-Accelerators and Beams* **18**, 050101.

Tomaschko C, Schurr M, Berger R, Saemann-Ischenko G, Voit H, Brunelle A, Della-Negra S and LeBeyec Y (1995) Visualization of craters in a Langmuir－Blodgett film from the impact of 23 MeV C ions. *Rapid Communications in Mass Spectrometry* **9**, 924–926.

Tomita S, Murakami M, Sakamoto N, Ishii S, Sasa K, Kaneko T and Kudo H (2010) Reduction in the energy loss of 0.5-MeV-per-atom carbon-cluster ions in thin carbon foils. *Physical Review A* **82**, 044901.

Whetten RL, Cox DM, Trevor DJ and Kaldor A (1985) Correspondence between electron binding energy and chemisorption reactivity of iron clusters. *Physical Review Letters* **54**, 1494.

Yamada I, Matsuo J, Toyoda N and Kirkpatrick A (2001) Materials processing by gas cluster ion beams. *Materials Science and Engineering: R: Reports* **34**, 231–295.